

# Present status of radiometric quality silicon photodiodes

R Korde<sup>1</sup>, C Prince<sup>1</sup>, D Cunningham<sup>2</sup>, R E Vest<sup>3</sup> and E Gullikson<sup>4</sup>

<sup>1</sup> International Radiation Detectors, Torrance, CA 90505-5243, USA

<sup>2</sup> Eastman Kodak Company, Rochester, NY 14653-9521, USA

<sup>3</sup> National Institute of Standards and Technology, Gaithersburg, MD 20899-8411, USA

<sup>4</sup> Center for X-Ray Optics, Materials Sciences Division, Lawrence Berkeley National Labs, Berkeley, CA 94720, USA

E-mail: rajkorde@ird-inc.com

Published 7 February 2003

Online at [stacks.iop.org/Met/40/S145](http://stacks.iop.org/Met/40/S145)

## Abstract

Evaluation of five types of silicon photodiode was undertaken to verify their suitability for absolute radiometry and also for their use as transfer standards in the spectral region from 1 nm to 1100 nm. Four types of photodiode were fabricated for this study; these were the p-on-n photodiode, n-on-p photodiodes with silicon dioxide front windows and n-on-p photodiodes with a metal-silicide front window. Fabrication of photodiodes with 100% internal quantum efficiency is demonstrated and their necessity for making absolute radiometric measurements with the lowest possible uncertainty is pointed out. The linearity characteristics of these devices, as measured by the ac/dc method, are far superior to those of the p-on-n diodes especially fabricated for this work and also to those exhibited by p-on-n diodes widely used at present by the radiometric community. Results on the stability of the quantum efficiency of the fabricated diodes after exposure to intense radiation of 13 nm, 120 nm, 157 nm, 193 nm and 254 nm radiation will also be presented. Photodiodes with a metal-silicide front window were the only devices stable when exposed to the intense beams of third-generation synchrotrons and UV excimer lasers.

## 1. Introduction

Silicon photodiodes with acceptable radiometric characteristics were selected for this study to further characterize them for all relevant parameters. The major goal of this work was to determine photodiode parameters affecting measurement uncertainty. The use of a silicon photodiode with a calibration traceable to a primary standard is attractive because the present primary standards, usually cryogenic radiometers, are expensive to purchase and operate.

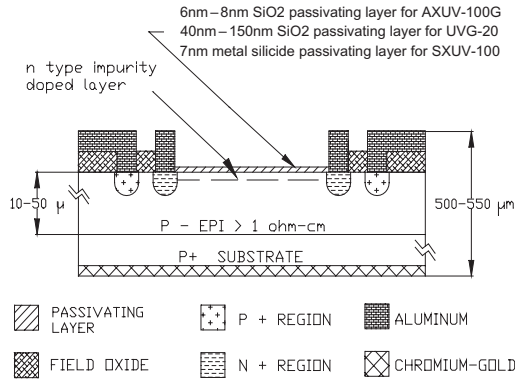
## 2. Photodiode structures

Four types of silicon photodiode were fabricated: n-on-p devices with thin oxide for the range 1 nm to 140 nm (AXUV-100G), n-on-p devices with thick oxide for the range 140 nm to 700 nm (UVG-20), p-on-n devices to cover the range 650 nm

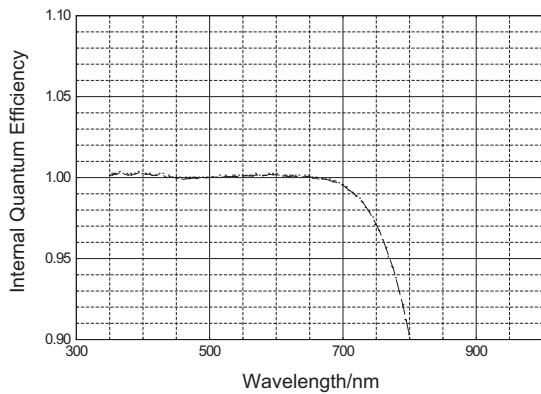
to 1100 nm (UVG-PN20) and silicide front window devices for the range 1 nm to 400 nm (SXUV-100). The active area of the fabricated UVG-20 and UVG-PN20 diodes is 5.5 mm in diameter and the active area of the AXUV-100G and the SXUV-100 diodes is 10 mm × 10 mm.

Figure 1 shows the structure of the UVG-20, AXUV-100G and SXUV-100 diodes. The UVG-PN20 diodes were made on n-type bulk wafers instead of the epitaxial wafers shown. A p-on-n photodiode widely used by the visible radiometric community from a different manufacturer (photodiode 'A') was included in this study for comparison. This device is also made on n-type bulk wafers.

The above photodiodes were evaluated for their quantum efficiency, stability, response linearity, and their suitability to make pulse energy measurements. Responsivity uniformity was evaluated for the SXUV photodiodes but it was omitted here for the AXUV and UVG diodes because of the well published work by other researchers [1–3].



**Figure 1.** Structure of the UVG-20, SXUV-100 and AXUV-100G photodiodes.



**Figure 2.** IQE of the UVG-20 photodiode.

### 3. Quantum efficiency

One unique property of the n-on-p photodiodes with passivating oxide window is the absence of a surface dead region, i.e. no photogenerated carrier recombination occurs in the doped n-type region or at the silicon-silicon dioxide interface. The absence of a dead region yields complete collection of carriers generated by ultraviolet (UV) and visible photons, resulting in 100% collection efficiency, as shown in figure 2. The internal quantum efficiency (IQE) measurements on the UVG-20 photodiode were performed using an ultraviolet to infrared Spectral Comparator Facility. This is an Optronic Labs<sup>5</sup> monochromator-based system that can measure the absolute spectral responsivity and spectral reflectance of photodiodes in the spectral region 190 nm to 2600 nm. The IQE below 350 nm was not reported here due to a discrepancy between the measured values and previously reported values [3]. The measurement error was due to low reflected light intensity when making the reflectance measurement below 350 nm.

Figure 3 compares the mean of three measurements of the internal quantum deficiency (1 minus the IQE) of two different UVG-20 photodiodes with the estimated uncertainties

<sup>5</sup> Certain commercial equipment, instructions or materials are identified in this article to foster understanding. Such identification does not imply recommendation or endorsement by the National Institute of Standards and Technology, National Institute of Health or by the US Department of Energy, nor does it imply that the materials or equipment identified are necessarily the best available for the purpose.

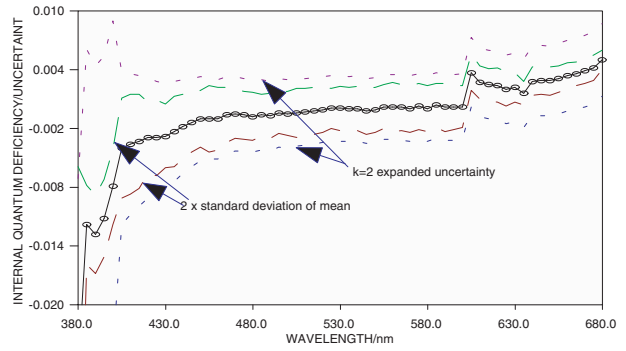


**Figure 3.** Measurement uncertainty for the UVG-20 photodiode.

determined from an analysis of a number of reflectance and relative quantum efficiency measurements carried out on these and other photodiodes. The average of the three experimental internal quantum deficiency spectra for the first UVG-20 photodiode differed from the average of the three experimental quantum deficiency spectra for the second photodiode by about 0.4% over the entire spectral range shown in figure 3. This fact is indicated by the curves showing plus and minus twice the standard deviation for the mean in figure 3. This type of systematic offset, which was observed throughout the measurements, is the major contributor to the  $k = 2$  estimated uncertainty limits shown in figure 3. The source of this wavelength-independent offset is unknown, but it occurred only rarely during a set of measurements, it was obvious in the data analysis, and the measurements were discarded and repeated at a later time. The cause of the spike in the internal quantum deficiency spectra for all of the photodiodes measured is unknown. However, since it is not consistent with the physical mechanisms that determine the IQE, it can be ruled out as unreal.

### 4. Stability of responsivity

Silicon n-on-p diodes with nitrided oxide layers are known to exhibit unsurpassed radiation hardness [4].

These devices show less than 2% responsivity degradation after exposure to several megajoules per square centimetre of 254 nm wavelength radiation and tens of kilojoules per square centimetre of 193 nm wavelength radiation.

It is known that the UV exposure-induced instability in the quantum efficiency of silicon photodiodes is related to the silicon dioxide window [4, 5]. The metal-silicide window in the SXUV series photodiodes replaces the SiO<sub>2</sub> window, thus eliminating the UV exposure-induced instability. Stability tests showed that the SXUV diodes exhibit less than 2% change in responsivity after receiving billions of 10 μJ cm<sup>-2</sup> pulses from both 193 nm and 157 nm excimer lasers.

Figure 4 shows the stability of responsivity of the SXUV-100 diode compared to the AXUV-100G diode when exposed to 100 eV photons with 3 × 10<sup>14</sup> photons s<sup>-1</sup> cm<sup>-2</sup> (5 mW cm<sup>-2</sup>) flux. After receiving a total fluence of 1.8 × 10<sup>18</sup> photons (29 J), the AXUV-100G diode showed approximately 28% decrease in response while the SXUV-100 diode showed virtually no change after the same exposure. Further exposure indicated that no change in the responsivity of the SXUV-100

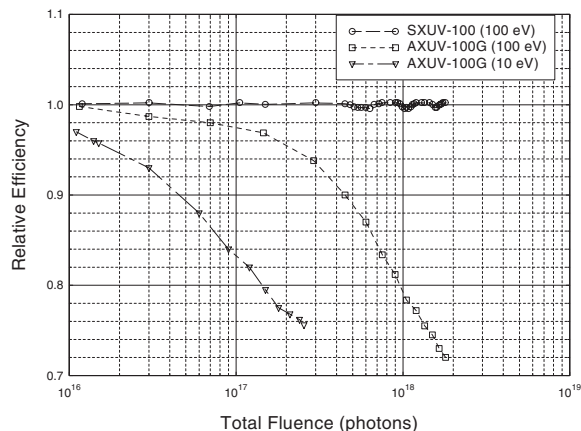


**Figure 4.** Relative responsivity of the SXUV-100 and AXUV-100G photodiodes when exposed to 100 eV and 10 eV photons.

diode is noticed after receiving a total fluence of  $10^{22}$  photons (160 kJ). Figure 4 also shows the stability of responsivity of the AXUV-100G diode when exposed to 10 eV photons with  $5 \times 10^{13}$  photons  $s^{-1} cm^{-2}$  ( $80 \mu W cm^{-2}$ ) flux. Again, virtually no change in the responsivity of the SXUV-100 diode was noticed after several hours of this exposure.

### 5. Uniformity of responsivity

The uniformity of responsivity of SXUV photodiodes with a  $1 cm \times 1 cm$  active area (model #SXUV-100) and a metal silicide front window was found to be within  $\pm 2\%$  when tested at 254 nm, 162 nm, 120 nm and 10 nm. Figure 5 shows the uniformity of spatial responsivity for the SXUV-100 photodiode at 121.6 nm with 1 mm diameter beam.

### 6. Linearity

Figure 6 shows the linearity of the UVG-20 photodiode and photodiode 'A' when exposed to increasing levels of 430 nm radiation. The standard ac/dc method was used to measure linearity [6]. Photodiode 'A' showed a noticeable decrease in responsivity at photocurrents greater than  $500 \mu A$  while the UVG-20 photodiode showed only 0.02% decrease in responsivity at a photocurrent of 3 mA.

The above non-linearity effect can be explained from the diode  $I-V$  equation:

$$I_T = I_L - I_0 \left[ \exp \left( \frac{eV_d}{nkT} \right) - 1 \right], \quad (1)$$

where,  $I_T$  is the current seen by an external circuit,  $I_L$  is the light-generated current,  $V_d$  is the forward voltage across the diode, and  $I_0$ ,  $n$ ,  $k$ ,  $T$  and  $q$  are the standard parameters of the diode equation (see e.g. [7]). Figure 7 shows the equivalent circuit of an illuminated photodiode. Under illumination,  $I_T$  becomes large and produces a voltage drop across  $R_s$  and  $R_L$ . This voltage is  $V_d$ , and its direction is such that it causes forward injection to occur in the diode, which reduces the net current to the load. This can be seen by rewriting equation (1) as

$$I_T = I_L - I_0 \left\{ \exp \left[ \left( \frac{eI_T}{nkT} \right) (R_s + R_L) \right] - 1 \right\}. \quad (2)$$

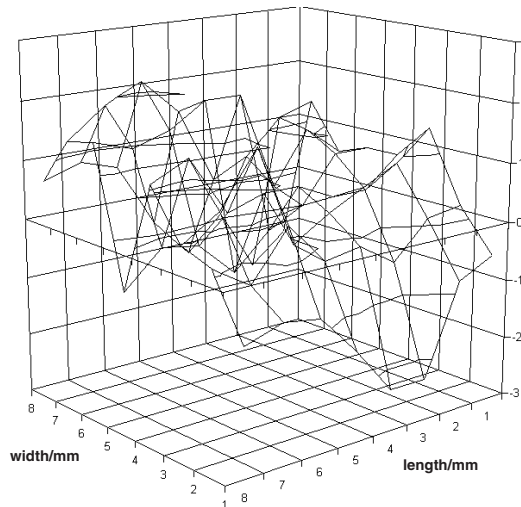


**Figure 5.** Spatial responsivity uniformity ( $\times 100$ ) of the SXUV-100 photodiode at 121.6 nm.

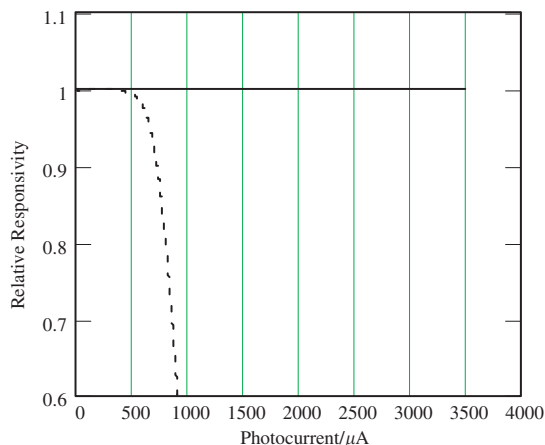


**Figure 6.** Linearity of the UVG-20 photodiode (—) and photodiode 'A' (- - -) when tested at 430 nm.

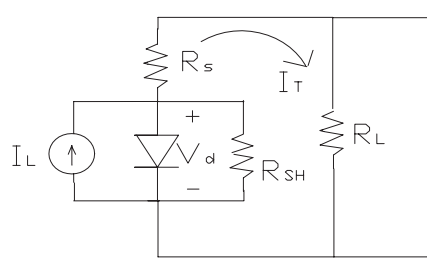


**Figure 7.** DC equivalent circuit of the illuminated photodiode.  $R_s$  and  $R_{sh}$  are the internal series and parallel resistances of the diode and  $R_L$  is the load resistance.

So it is the series resistance and the load resistance that determine the linear range for a photodiode (see also [8]).

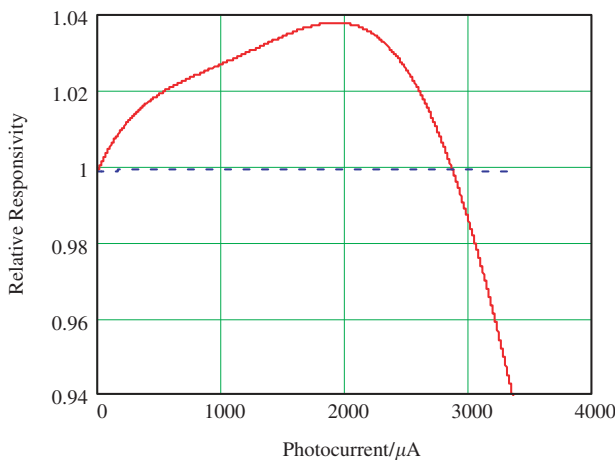
Note that we have neglected any current flow through the diode shunt resistance  $R_{sh}$  because this resistance, typically  $\sim 1 G\Omega$ , is much larger than either  $R_s$  or  $R_L$ .

From the device parameters of the UVG-20 diode (estimated  $R_s = 90 \Omega$ , measured  $I_0 = 2.7 \times 10^{-11} A$ ) and using a  $10 \Omega$  load resistance, the calculated loss in responsivity is 0.09% at 3 mA. The discrepancy between the calculated

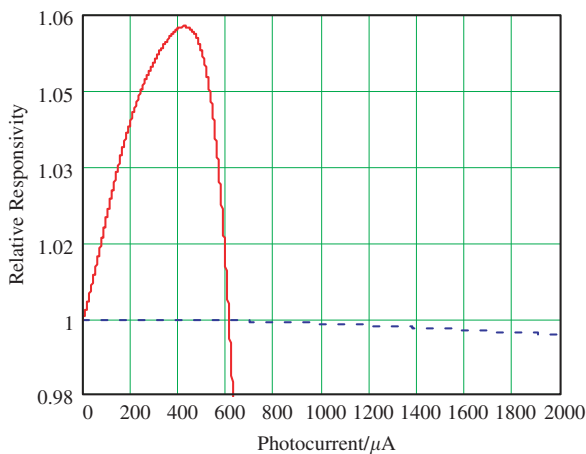
and measured values is mostly attributed to the estimation of the series resistance of the UVG-20 photodiode. From the measured value of linearity, it is estimated that photodiode 'A' had a series resistance of about 700 Ω.

Figure 8 shows the linearity of a p-on-n photodiode which has an IQE of 80% at 430 nm. This low IQE is a result of photogenerated carrier recombination in the front region. The supralinearity (increased responsivity) is caused by the filling of trap centres with increasing flux. As the trap centres are filled, the minority carrier lifetime increases, which reduces the photogenerated carrier recombination and increases the responsivity. The UVG-20 photodiode has 100% IQE (no photogenerated carrier recombination) at 430 nm so it does not show supralinearity.

Figure 9 compares the linearity of the UVG-20 photodiode and photodiode 'A' when exposed to increasing levels of 980 nm radiation. Photodiode 'A' showed significant supralinear behaviour for photocurrents above 20 μA while no noticeable supralinearity was observed in the UVG-20 diode. At high irradiance levels, photodiode 'A' was found to lose responsivity much more rapidly than the UVG-20 diode because of the high series resistance associated with this diode.



**Figure 8.** Relative response of a p-on-n photodiode with 80% IQE (—) and the UVG-20 photodiode with 100% IQE (- - -) at 430 nm.



**Figure 9.** Linearity of the UVG-20 (- - -) and photodiode 'A' (—) when tested at 980 nm.

Interestingly, the linearity of the p-on-n diodes specially fabricated for this work (UVG-PN20) was exactly the same as that of the standard UVG-20 diode depicted in figure 9. Also, the internal quantum efficiencies of the UVG-PN20 and photodiode 'A' are nearly equivalent at 980 nm, indicating that they have the same minority carrier lifetime. This suggests that the minority carrier lifetime (diffusion length) is not the only factor which determines the supralinearity, as was previously believed [9].

The dopant concentration in the n-type region of the UVG-PN20 photodiode is  $2 \times 10^{13} \text{ cm}^{-3}$  and that of photodiode 'A' is  $5 \times 10^{12} \text{ cm}^{-3}$ . Computer modelling qualitatively predicts the observed difference in supralinearity as a result of the dopant concentrations in the starting material. Because it is difficult to correct for non-linearity errors, high accuracy applications require linear photodiodes.

### 7. Pulse responsivity

An MPB 193 nm excimer laser (model #PSX-100) was used to compare the pulse responsivity of UVG-100 and SXUV-100 diodes and their measured cw responsivities. The pulse duration of the PSX-100 is 10 ns. Attenuators were used to reduce the 3 mJ pulse energy of the PSX-100 to the pulse energies shown in table 1. A capacitively coupled bias tee (IRD model BT-250) was used to reverse bias the detectors up to 120 V. The photodiode voltage as a function of time  $V(t)$  was measured with a LeCroy 500 MHz digital oscilloscope with 50 Ω input impedance  $R$  and the charge  $Q$  created in the photodiode per pulse was calculated as

$$Q = \frac{1}{R} \int V dt. \tag{3}$$

This integral was evaluated using the oscilloscope's built-in area function. The pulse energy of the PSX-100 was measured with an Ophir Laserstar with PE10 pyroelectric detector head, which has an uncertainty of approximately 10% with 2 μJ incident pulse energy at 193 nm.

The pulse responsivity (charge generated per unit energy incident) was calculated by dividing the measured charge created in the detector by the measured pulse energy. As seen in table 1, the correlation between the cw and pulsed 193 nm response agrees with previous results for visible wavelengths [10]. This experimental verification that the cw responsivity can be used to measure pulse energy is critical to radiometric measurements of 157 nm and 13 nm pulses, for which no primary standard is available at present.

### 8. Conclusion

Important parameters that govern performance of the radiometric quality silicon photodiodes are identified. It has been shown that the non-linear behaviour of the photodiodes in the ultraviolet as well as in the near infrared should be known before they are used as absolute devices or radiometric transfer standard detectors. Devices with 100% IQE are the ideal radiometric devices because they do not exhibit the supralinear behaviour. The experimental correlation between the cw and pulse responsivity is important for the measurement of deep ultraviolet and extreme ultraviolet pulsed sources because no primary standards for pulsed radiation are currently available.

**Table 1.** Comparison of cw and pulse responsivity of UVG series and SXUV series photodiodes when exposed to 100 nJ, 1  $\mu$ J and 2.5  $\mu$ J pulses with a 3 mm diameter beam. Because of the high responsivity, the UVG diode was saturated at the 2.5  $\mu$ J/pulse energy level.

Device	cw responsivity at 193 nm	Responsivity for 193 nm pulse radiation					
		100 V reverse bias			120 V reverse bias		
		100 nJ	1 $\mu$ J	2.5 $\mu$ J	100 nJ	1 $\mu$ J	2.5 $\mu$ J
UVG-100 00-26	0.137 A W <sup>-1</sup>	0.127 C J <sup>-1</sup>	0.122 C J <sup>-1</sup>	sat	0.129 C J <sup>-1</sup>	0.123 C J <sup>-1</sup>	sat
SXUV-100 02-2	0.0104 A W <sup>-1</sup>	0.0101 C J <sup>-1</sup>	0.0108 C J <sup>-1</sup>	0.0105 C J <sup>-1</sup>	0.0102 C J <sup>-1</sup>	0.0108 C J <sup>-1</sup>	0.0105 C J <sup>-1</sup>

### Acknowledgments

This work was supported in part by grant No 5 R44 GM47180-03 from the US National Institute of Health and grant No DE-FG03-96ER82190 from the US Department of Energy. We wish to thank Dr Jon Geist for providing the uncertainty analysis for the IQE measurements.

### References

- [1] Shaw P, Larason T C, Gupta R, Brown S W, Vest R E and Lykke K 2001 *Rev. Sci. Instrum.* **72** 2242–7
- [2] Larason T C and Bruce S S 1998 *Metrologia* **35** 491–6
- [3] Canfield L R, Vest R E, Korde R, Schmidtke H and Desor R 1998 *Metrologia* **35** 329–34
- [4] Korde R, Cable J and Canfield R 1993 *IEEE Trans. Nucl. Sci.* **40** 1655–9
- [5] Korde R and Geist J 1987 *Appl. Opt.* **26** 5284–90
- [6] Frehlich R 1992 *Appl. Opt.* **31** 5926–9
- [7] Edward S Yang 1988 *Microelectronic Devices* (New York: McGraw-Hill) p 360
- [8] Chaffin R J and Osbourn G C 1980 *Appl. Phys. Lett.* **37** 637–9
- [9] Schaefer A R, Zalewski E F and Geist J 1983 *Appl. Opt.* **22** 1232–5
- [10] Stuik R and Bijkerk F 2002 *Nucl. Instrum. Methods A* **489** 370–8